

Article

The Activity Enhancement Effect of Ionic Liquids on Oxygen Reduction Reaction Catalysts: From Rotating Disk Electrode to Membrane Electrode Assembly

Kan Huang ¹, Oscar Morales-Collazo ², Zhichao Chen ², Tangqiumei Song ², Liang Wang ¹, Honghong Lin ¹, Joan F. Brennecke ^{2,*} and Hongfei Jia ^{1,*}

¹ Toyota Research Institute of North America, 1555 Woodridge Ave., Ann Arbor, MI 48105, USA; khuang0207@gmail.com (K.H.); liang.wang@toyota.com (L.W.); honghong.lin@toyota.com (H.L.)

² McKetta Department of Chemical Engineering, The University of Texas at Austin, 200 E Dean Keeton St, Austin, TX 78712, USA; omcquim@gmail.com (O.M.-C.); zhichaochen@utexas.edu (Z.C.); tangsong@utexas.edu (T.S.)

* Correspondence: jfb@che.utexas.edu (J.F.B.); hongfei.jia@toyota.com (H.J.)

Abstract: Ionic liquids (ILs) have been explored as a surface modification strategy to promote the oxygen reduction reaction (ORR) on Pt/C and their chemical structures were identified to have strong influence on the ORR activities. To better understand the roles of anion and cation of ILs on the catalytic reaction, two cations ([MTBD]⁺ and [bmim]⁺) were paired with three anions ([TFSI]⁻, [beti]⁻, and [C₄F₉SO₃]⁻) to form various IL structures. By systematically varying the IL combinations and studying their effects on the electrochemical behaviors, such as electrochemical surface area and specific ORR activities, it was found that cation structure had a higher influence than anion, and the impact of the [MTBD]⁺ series was stronger than the [bmim]⁺ series. In addition to the investigation in the half-cell, studies were also extended to the membrane electrode assembly (MEA). Considerable performance enhancements were demonstrated in both the kinetic region and high current density region with the aid of IL. This work suggests that IL modification can provide a complementary approach to improve the performance of proton exchange membrane fuel cells.

Keywords: polymer electrolyte membrane fuel cells; membrane electrode assembly; cathode catalyst; oxygen reduction reaction; ionic liquid



Citation: Huang, K.; Morales-Collazo, O.; Chen, Z.; Song, T.; Wang, L.; Lin, H.; Brennecke, J.F.; Jia, H. The Activity Enhancement Effect of Ionic Liquids on Oxygen Reduction Reaction Catalysts: From Rotating Disk Electrode to Membrane Electrode Assembly. *Catalysts* **2021**, *11*, 989. <https://doi.org/10.3390/catal11080989>

Academic Editors: Tao Huabing and Hongbin Yang

Received: 2 August 2021

Accepted: 14 August 2021

Published: 18 August 2021

Publisher's Note: MDPI stays neutral with regard to jurisdictional claims in published maps and institutional affiliations.



Copyright: © 2021 by the authors. Licensee MDPI, Basel, Switzerland. This article is an open access article distributed under the terms and conditions of the Creative Commons Attribution (CC BY) license (<https://creativecommons.org/licenses/by/4.0/>).

1. Introduction

Polymer electrolyte membrane fuel cells (PEMFCs) along with hydrogen from renewable sources provide an important path to global carbon neutrality. After decades of technological advances, the commercialization of PEMFCs has expanded rapidly from personal owned vehicles to a wide variety of uses, including mid-to-heavy duty trucks, train, maritime uses, aviation, stationary power for data centers, etc. [1]. For many of these emerging applications, the fuel cell operational efficiency, which directly affects the total cost of ownership, continues to be the center of material research and technology development. As the oxygen reduction reaction (ORR) on the cathode accounts for significant energy loss, intensive efforts have been dedicated to research on various kinds of Pt based catalyst materials, represented by Pt-alloy, core-shell and shape-controlled catalysts [2–4]. Modification of catalyst surface with additives such as ionic liquid (IL) has been also proposed as a complementary approach to the further enhancement of catalyst performance. Snyder et al. [5] first reported that the encapsulation of nanoporous PtNi with IL significantly boosts its ORR activity in a rotating disk electrode (RDE) configuration. Such a strategy was also applied later to a nanoframe-type of high performance PtNi catalyst and achieved more than 50% of enhancement of mass activity at 0.95 V in 0.1 M HClO₄ [6]. Etzold et al. also reported a positive shift of ORR polarization curve

and an increase of activity after impregnating Pt nanoparticles [7,8] and octahedral shape-controlled catalysts with IL [9]. As to the possible mechanism of such a promotional effect of IL, it has been suggested that IL increases the oxygen concentration at the Pt interface and reduces the undesired side reactions such as the oxygenated species formation (e.g., OH_{ads}) [5]. The former increases the collision frequency between oxygen and Pt surface, and the latter lowers the barrier to initiating the reaction [5,8,10–12]. In a catalyst layer, where perfluorosulfonic acid (PFSA)-based ionomers are used as the binder, IL may also help mitigate the anion adsorption/poisoning effect on Pt-based catalysts [13].

Several types of ILs have been studied, such as 7-methyl-1,5,7-triazabicyclo [4.4.0] dec-5-ene[bis(perfluoroethylsulfonyl)imide] ([MTBD][beti]) [5,10] and 1-butyl-3-methylimidazolium bis(trifluoromethylsulfonyl)imide ([bmim][TFSI]) [8]. Erlebacher et al. [11] investigated several combinations of cation and anion to examine their effects on electrochemical performances such as ORR activity and electrochemical surface area (ECA). When switching cation structure from [MTBD]⁺ to [bmim]⁺ with the same anion (e.g., [beti][−]), it was found that [MTBD][beti] modified Pt exhibited a much smaller ECA than [bmim][beti]. On the other hand, changing the anion structure from [beti][−] to [TFSI][−] resulted in a decrease of ORR activity. Their results suggested that the anion and cation may affect the reaction process differently. Recently, the effect of cationic chain length was investigated with a series of 1-methyl-3-alkylimidazolium bis-(trifluoromethanesulfonyl)imides ([C_nC₁im][NTf₂], n = 2–10) [14]. It has been found that the longer length of the side chain might help depress the formation of nonreactive oxygenated species, but also block active sites and lead to a lower electrochemically active surface area.

The primary goal of this work is to explore the roles of cation and anion on the electrochemical performance of the catalysts and provide additional insights for the future design of IL structures. To do so, combinations of two cations and three anions were constructed and they are shown schematically in Figure 1. We previously studied the effect of IL on the ORR activity at high IL loadings (i.e., over 50 wt.%) and found a substantial leaching of IL into the electrolyte [12]. Only the remaining IL was assumed to act as the ORR promoter. Therefore, in this study we investigated a series of ILs at a lower loading in both RDE and MEA to avoid excess use of IL. In addition to the routine electrochemical analysis such as cyclic voltammetry and linear sweep voltammetry, measurements using CO displacement and CO stripping were also employed. The principal of CO displacement is that CO replaces the initially adsorbed ions on Pt and induces displacement charges [15]. Our previous work reported that IL incorporated Pt/C showed less displacement charge than IL free Pt/C, assuming that IL reduced the anion adsorption on Pt (e.g., sulfonate ion (−SO₃H) of ionomer) [12]. Therefore, comparing the displacement charges of various Pt/C-ILs systems might be informative to examine the interaction of ILs with Pt. CO stripping not only provides an estimation of ECA [16,17], but also the surface information of Pt such as Pt-oxides formation (e.g., OH_{ads}) [18]. In the Pt-ILs systems, the decrease of ECAs was usually accompanied by the reduction of Pt-oxides formation [7,10–12]. As a result, the examination of the CO stripping process on Pt-ILs may reveal the mechanism.

To advance the application of the IL surface modification strategy towards practical application, it is necessary to extend the RDE-based fundamental studies to investigations at the MEA level. After the earlier demonstration of MEA performance improvement with the IL-modified nanoporous PtNi catalyst [10], it seems to be quite challenging to re-validate such an observation on other type of catalysts. It has been hypothesized that randomly deposited IL coating on the catalyst with various thickness might block certain pores of the catalyst layer and thus hinder mass transport. To overcome such an issue, a sequential capacitive deposition method was developed to obtain thin, conformal IL coating (<2 nm) on the surface of Pt/C ORR catalysts [19]. While the catalyst performance improvement was observed again in the half-cell setup, the effectiveness of this strategy for MEA remains to be proven. The only other study that reported MEA performance improvement involved the use of a mixture of Nafion and a sulfonated poly(ionic liquid) block copolymer as the ionomer binder, from which enhancement was seen in both the kinetic and mass

transport-limited regions [20]. In the later part of this study, we extended the investigation to MEAs, focusing on the effects of IL loading, the ink formula, and catalyst property on the performance. With a careful balance of those parameters, considerable performance improvement was demonstrated.

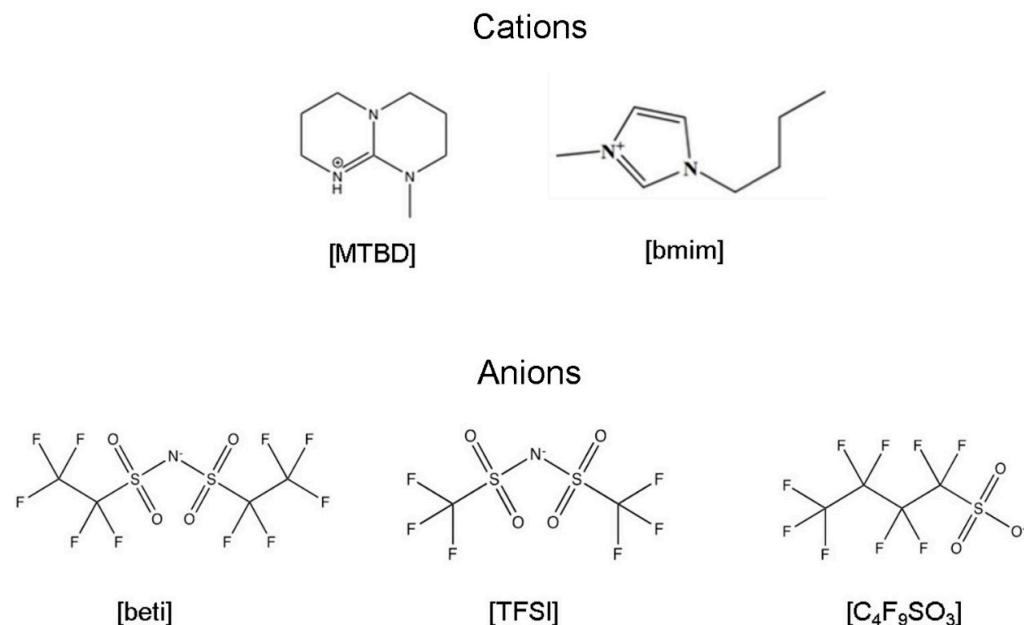


Figure 1. Chemical structure of the IL anions and cations studied in this work.

2. Results and Discussion

The IL synthesis routes were well established, and the purities were confirmed by NMR [12] (see Supplementary Information for the NMR spectra). ATR-FTIR spectra of [bmim][beti], [bmim][TFSI] and [MTBD][beti] were shown in Figure 2. The main differences, such as the $-C-C-F$ bond in [beti][−] and the $-C=C-$ bond in [MTBD]⁺, are indicated in the figure. The Pt/C was incorporated with various ILs and their cyclic voltammograms are shown Figure 3. The addition of hydrophobic ILs reduced the anodic charge in the Pt oxidation region and the hydrogen adsorption charge under the H_{upd} region, which has been previously observed [8,10–12]. One interesting finding is that the hydrogen adsorption profiles of the [bmim]⁺ series are identical, but smaller than that of the [MTBD]⁺ series. It seems that the cation imposes more influence on the amount of hydrogen adsorption than the anion. There are several hypotheses regarding the decrease of $ECA(H_{\text{upd}})$. Arras et al. [21] studied the hydrogen adsorption on ionic liquid coated palladium (Pd) particles and found that the anion structure affects the hydrogen uptake very much. It is suggested that the anion interacts with the Pd and changes the accessibility of Pd sites for the following hydrogen adsorption. To the contrary, our results (Figure 3) showed that the anion structure did not change the $ECA(H_{\text{upd}})$ very much. For instance, the three [bmim]⁺ ILs exhibited virtually identical hydrogen adsorption behaviors. Another hypothesis proposed is that IL molecules prevent hydrogen adsorption by occupying certain of the metal facets [7]. In Figure 3, hydrogen shows a sharp adsorption on Pt(110) in the perchloric acid [22]. After incorporating [bmim]⁺ ILs, the signature hydrogen adsorption peaks remained, only with reduced areas. In contrast, the adsorption peak became broader and less shaped after the incorporation of [MTBD]⁺ ILs. It is speculated that [MTBD]⁺ ILs may inhibit the hydrogen adsorption on Pt(110), presumably owing to a stronger bond of [MTBD]⁺ on Pt than [bmim]⁺.

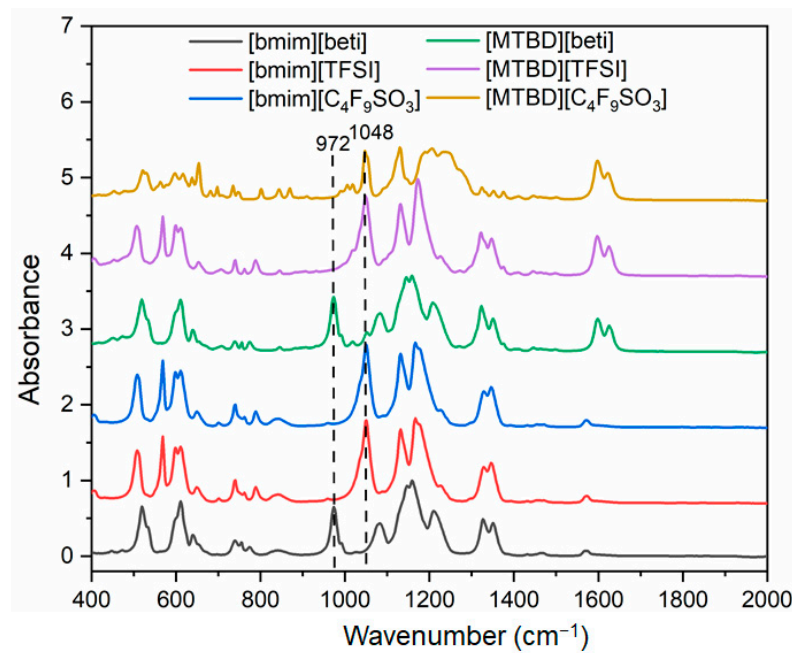


Figure 2. ATR-FTIR spectra of [bmim][beti], [bmim][TFSI], [bmim][C₄F₉SO₃], [MTBD][beti], [MTBD][TFSI] and [MTBD][C₄F₉SO₃].

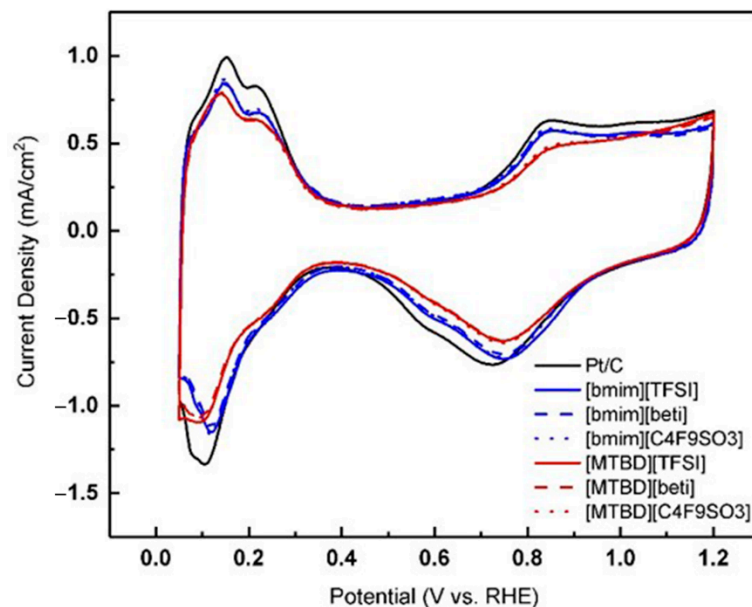


Figure 3. Cyclic voltammograms of Pt/C (Johnson Matthey Hispec 3000) and Pt/C-ILs in N₂-saturated 0.1 M HClO₄. Scan rate: 50 mV·s⁻¹ and the Pt loading was 16.2 ug/cm²_{disk}.

To further elucidate the mechanism of the decrease of ECA(H_{upd}) and investigate how the ILs alter the hydrogen adsorption, a CO stripping measurement was conducted as an alternative approach to estimate the accessible Pt sites. Figure 4a displays an example of CO stripping voltammetry of Pt/C-ILs, which showed identical oxidation profiles to Pt/C, but with a positive shift of the main peak position. More discussion regarding the peak shift and its effect on the ORR activity will be detailed subsequently. The charge under the CO oxidation peak was used to calculate the ECA(CO). Figure 5a,b display the comparison of ECA(CO) and ECA(H_{upd}) with incorporation of [bmim]⁺ and [MTBD]⁺ ILs, respectively. Compared to Pt/C, Pt/C-ILs both showed smaller ECA(CO) and ECA(H_{upd}). Meanwhile, the ratios of ECA(CO)/ECA(H_{upd}) of Pt/C-ILs were close to 1. Since the measurements of ECA(CO) and ECA(H_{upd}) assumed that adsorbed CO and hydrogen forms a monolayer on

the Pt surface, it is reasonable to deduce that the decrease of $ECA_{(CO)}$ and $ECA_{(H_{upd})}$ may follow a similar mechanism. Arras et al. [21,23] studied the CO and H₂ uptake in an IL coated palladium composite. It was found that IL coating significantly decreased the CO and H₂ uptake, which was attributed to the low gas solubilities in IL and the competitive adsorption of gas molecules and IL ions. Here, we propose two possible mechanisms that may result in the decrease of ECA: (1) IL partially covers the Pt surface and reduces the direct exposure of active sites for the adsorption; and (2) the competing adsorption of IL ions and CO/hydrogen restricts their full adsorption on the IL covered Pt surface.

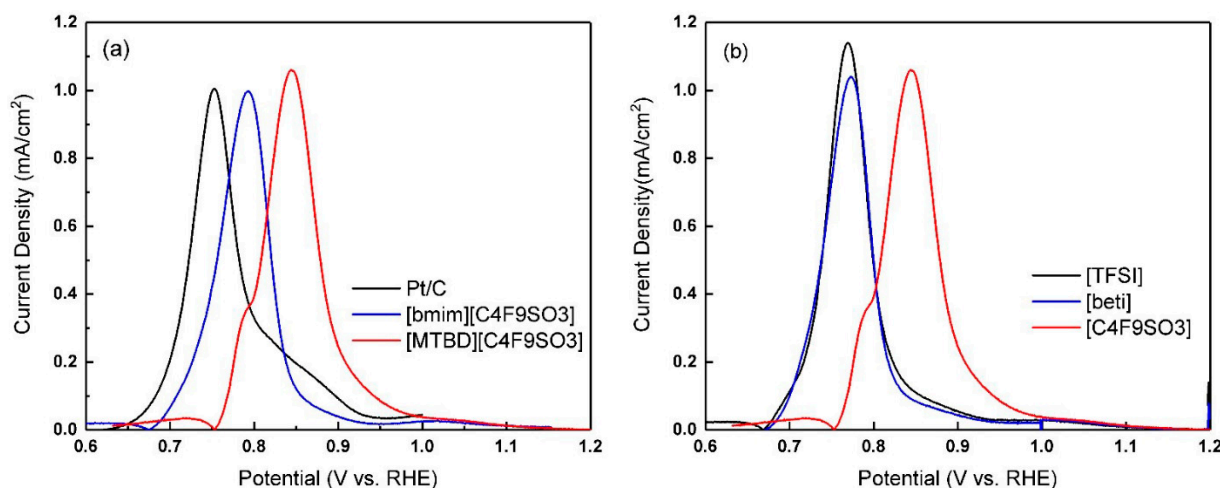


Figure 4. CO stripping measurements. (a) Stripping voltammograms of Pt/C, Pt/C-[bmim][C₄F₉SO₃], and Pt/C-[MTBD][C₄F₉SO₃]. (b) Stripping voltammograms of Pt/C-[MTBD][TFSI], [MTBD][beti], and [MTBD][C₄F₉SO₃].

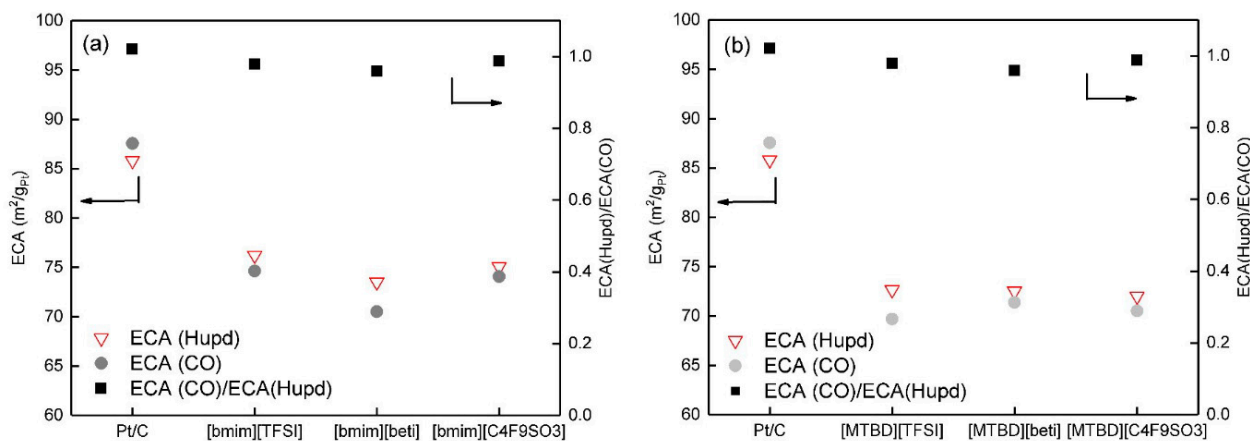


Figure 5. Comparison of electrochemical surface area of (a) [bmim]⁺ ILs and (b) [MTBD]⁺ ILs measured by CO stripping $ECA_{(CO)}$ and by hydrogen underpotential adsorption $ECA_{(H_{upd})}$. The right y-axis shows the ratio of $ECA_{(H_{upd})}/ECA_{(CO)}$.

Feliu et al. [24–27] developed an electrochemical method using CO as a probe molecule to study the ion adsorption on the Pt surface. The technique later evolved to be called “CO-displacement” and was adopted to semi-quantify ion coverage such as ionomer sulfonate ion (–SO₃H) coverage [15]. Basically, CO displaces the initially adsorbed species from Pt at a given potential and cation or anion is released from the Pt surface, inducing an oxidative or reductive current, respectively. The choice of potential is critical, because it determines which species are displaced. In general, at potentials lower than 0.3 V, the primary displaced species are the adsorbed hydrogen (cation). To displace the anion species, the potential is usually held at 0.4 V or 0.5 V [15]. In a supporting electrolyte (e.g., 0.1 M HClO₄), the hydrogen adsorption accounts for the majority of cation displacement charge, making the separation of the displacement charge of IL cation and atomic hydrogen very challenging.

Our previous study showed that IL forms a thin layer on Pt and restricts the anion adsorption (e.g., (bi)sulfate, SO_4^{2-}), resulting in a smaller displacement charge [12]. Therefore, CO displacement was conducted in the region where anion adsorption is dominant, and the displacement charge was used to examine the interaction between ILs and Pt.

Figure 6a displays the current responses after introduction of the CO gas. The negative current indicated that the released species were adsorbed anions and the integrated charge was the total amount of initially adsorbed anions. For Pt/C, the negative displacement charge is induced by the release of ionomer ($-\text{SO}_3\text{H}$) and adsorbed perchlorate ion (ClO_4^-), although perchlorate ion is thought to be non-adsorbing [15,28]. In the case of Pt/C-[MTBD][beti], the displacement charge is much smaller than Pt/C, suggesting less initially adsorbed anions on the surface. Although it is very challenging to distinguish the displacement charge of $[\text{beti}]^-$ from the perchlorate ion and ionomer, it is reasonable to deduce that the reduced displacement charge of Pt/C-[MTBD][beti] is due to less direct contact with the electrolyte or ionomer, or the mixture of both. The adsorption of $[\text{beti}]^-$ cannot be precluded. The anion species that can be displaced and the corresponding displacement charge depend on the selected potential. At potentials of 0.4 V and 0.5 V, the displacement charges of Pt/C were measured to be $-2.11 \text{ mA}\cdot\text{s}$ and $-2.08 \text{ mA}\cdot\text{s}$, suggesting that the adsorption of perchlorate ion and ionomer ($-\text{SO}_3\text{H}$) has saturated on the Pt surface at 0.4 V. In contrast, the displacement charges of Pt/C-[MTBD][beti] were $-1.31 \text{ mA}\cdot\text{s}$ at 0.4 V and $-1.69 \text{ mA}\cdot\text{s}$ at 0.5 V. This indicates that higher potential drives additional adsorption of anions, presumably originating from the $[\text{beti}]^-$ in [MTBD][beti]. As a result, the displaced anions of Pt/C-[MTBD][beti] are consisted of ClO_4^- , ($-\text{SO}_3\text{H}$), and $[\text{beti}]^-$. Unlike [MTBD][beti], Pt/C-[bmim][beti] exhibited a slightly higher displacement charge than Pt/C. Results shown in Figure 6a,b have evidenced the presence of [bmim][beti]. Therefore, it is assumed that the substantial adsorption of $[\text{beti}]^-$ outnumbered the reduced adsorption of perchlorate ion and ionomer, resulting in an increase of displacement charge. The lower displacement charge of Pt/C-[MTBD][beti] than Pt/C-[bmim][beti] indicates that [MTBD][beti] may have stronger interaction with Pt and restricts more anion adsorption, such as ClO_4^- and ($-\text{SO}_3\text{H}$).

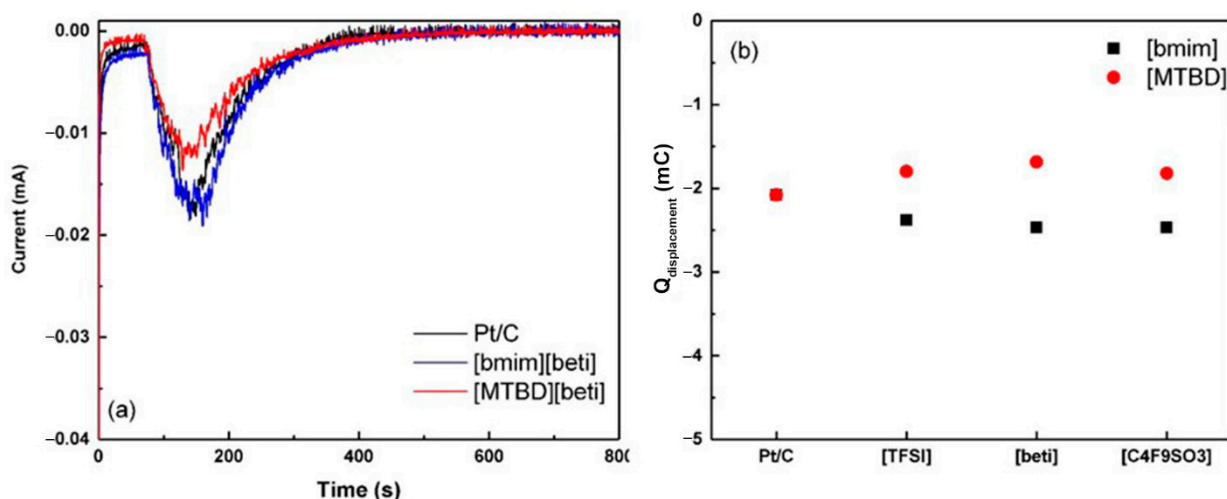


Figure 6. CO displacement characterization. (a) Current-time response after CO gas is introduced. (b) The summary of displacement charges of Pt/C and Pt/C-ILs. The potential was held constant at 0.5 V in air free 0.1 M HClO_4 .

The CO displacement for Pt/C with the full series of $[\text{bmim}]^+$ and $[\text{MTBD}]^+$ ILs were further measured, and the results are presented in Figure 4b. All three systems with $[\text{MTBD}]^+$ ILs had virtually identical displacement charges. Similarly, the $[\text{bmim}]^+$ series also showed identical displacement charges, but the values were higher than $[\text{MTBD}]^+$ ILs. This suggests that the cation imposes a higher impact on the interaction with Pt than the anion and $[\text{MTBD}]^+$ shows stronger interaction strength than $[\text{bmim}]^+$. The results along with the CV studies lead one to conclude that: The decrease of $\text{ECA}(\text{H}_{\text{upd}})$ and $\text{ECA}(\text{CO})$ is

due to IL covering Pt that restricts the direct adsorption of CO/hydrogen, and the cation structure affects the amount of CO/hydrogen adsorption through a competitive adsorption mechanism.

The study described above suggests the ILs with varied structures may interact with the catalyst differently. Therefore, contact angle measurements of ILs were carried out on a glassy carbon (GC) and a flat platinum film to study their affinities for the substrates. Examples of contact angles of [MTBD][TFSI] and [bmim][TFSI] on GC and Pt film are shown in Figure 7a–d. The contact angles of [MTBD][TFSI] are larger than that of [bmim][TFSI] on both GC and Pt film, suggesting a higher surface tension of [MTBD][TFSI]. The measurements were also conducted on the rest of ILs except for [MTBD][C₄F₉SO₃], which is a solid at room temperature. The results were summarized in Figure 7e. The [bmim]⁺ ILs have virtually identical contact angles on GC, and they are smaller than the [MTBD]⁺ ILs series. A similar trend of contact angles was also found on the Pt surface. Although the surface properties of GC and Pt film tested here are different from the Pt/C used for electrochemical measurements, which possesses high surface roughness, the contact angle measurements still provide indirect evidence towards the interaction between IL and catalyst. The results showed that the cation affected the interaction more than the anion, which is consistent with the findings in the electrochemical studies.

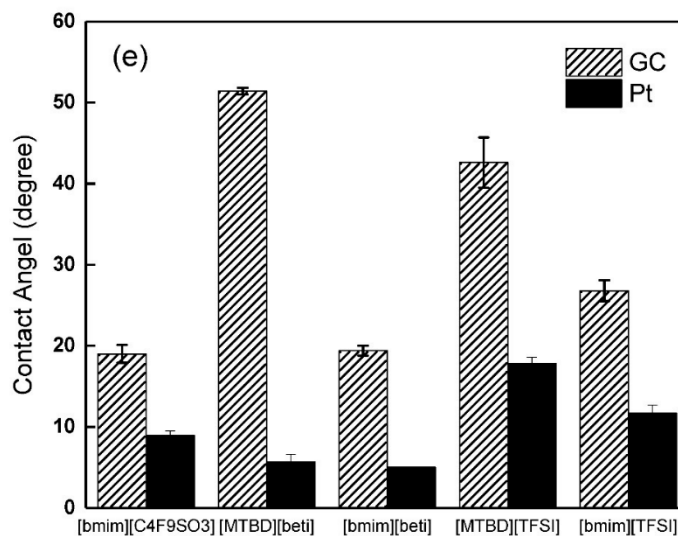
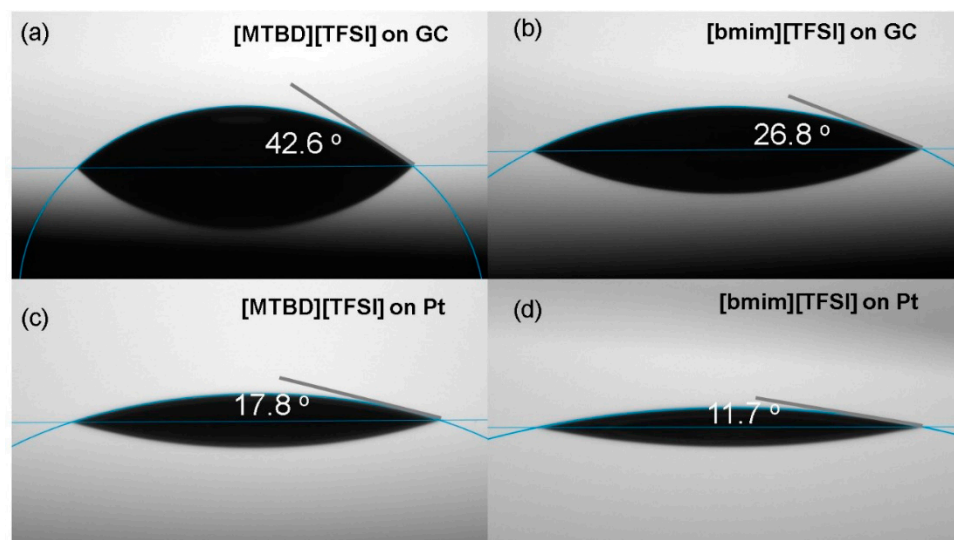


Figure 7. Contact angle measurements. (a) [MTBD][TFSI] on GC. (b) [bmim][TFSI] on GC. (c) [MTBD][TFSI] on Pt surface. (d) [bmim][TFSI] on Pt surface. (e) comparison of measured contact angles of all ILs except [MTBD][C₄F₉SO₃] which is solid at room temperature.

The formation of OH_{ads} on Pt through $\text{Pt} + \text{H}_2\text{O} \rightarrow \text{Pt-OH}_{\text{ads}} + \text{H}^+ + \text{e}^-$ is known to block the metallic Pt site and imposes a negative electronic effect on the ORR kinetics [29,30]. In the process of CO stripping, the reaction between adsorbed CO_{ads} and the adjacent formed OH_{ads} ($\text{CO} + \text{OH}_{\text{ads}} \rightarrow \text{CO}_2 + \text{H}^+ + \text{e}^-$) is generally considered to be the rate determining step [17,18]. With the aid of CO, it is possible to probe the effect of IL on the Pt- OH_{ads} formation. Representative CO stripping voltammograms for Pt/C and Pt/C-ILs are presented in Figure 4a. Compared to Pt/C, the main CO oxidation peak of Pt/C-ILs shifts towards a higher potential, indicating a delay of CO oxidation reaction caused by less OH_{ads} formation. Furthermore, the oxidation peak potential of [MTBD][$\text{C}_4\text{F}_9\text{SO}_3$] is higher than that of [bmim][$\text{C}_4\text{F}_9\text{SO}_3$]. It is presumed that the total amount of OH_{ads} formed on Pt/C-[MTBD][$\text{C}_4\text{F}_9\text{SO}_3$] was less than [bmim][$\text{C}_4\text{F}_9\text{SO}_3$]. Measurements were further extended to study the rest of the ILs, and an example of the [MTBD]⁺ ILs series is presented in Figure 4b. The peak potentials varied with the anion, and followed an order of $[\text{TFSI}]^- \approx [\text{beti}]^- < [\text{C}_4\text{F}_9\text{SO}_3]^-$. It is speculated that $[\text{C}_4\text{F}_9\text{SO}_3]^-$ restricts OH_{ads} formation the most, presumably owing to its long hydrophobic fluoroalkyl chain.

Representative ORR polarization curves of Pt/C-ILs are displayed in Figure 8a. Compared to Pt/C, the half wave potential of Pt/C-ILs were positively shifted by ~10 mV, reflecting enhanced ORR activities. A ~36% increase in the mass activity was achieved at 0.9 V. However, the difference of apparent current is small when comparing [MTBD][$\text{C}_4\text{F}_9\text{SO}_3$] to [bmim][$\text{C}_4\text{F}_9\text{SO}_3$]. Conway et al. [31] proposed that after Pt- OH_{ads} is initially formed, it will be subject to a “place-exchange” process, and finally inserted under the metal skin. Only the most recently formed Pt- OH_{ads} stays on the top of the Pt surface, and only this Pt- OH_{ads} is reversible, accounting for about 10% of the total surface oxygenated species. Moreover, chemisorbed O_{ads} instead of OH_{ads} is formed between 0.85 V and 1.15 V [32]. The CO stripping may only react with the reversible OH_{ads} on the top of Pt, but not the other oxygenated species within the Pt lattice.

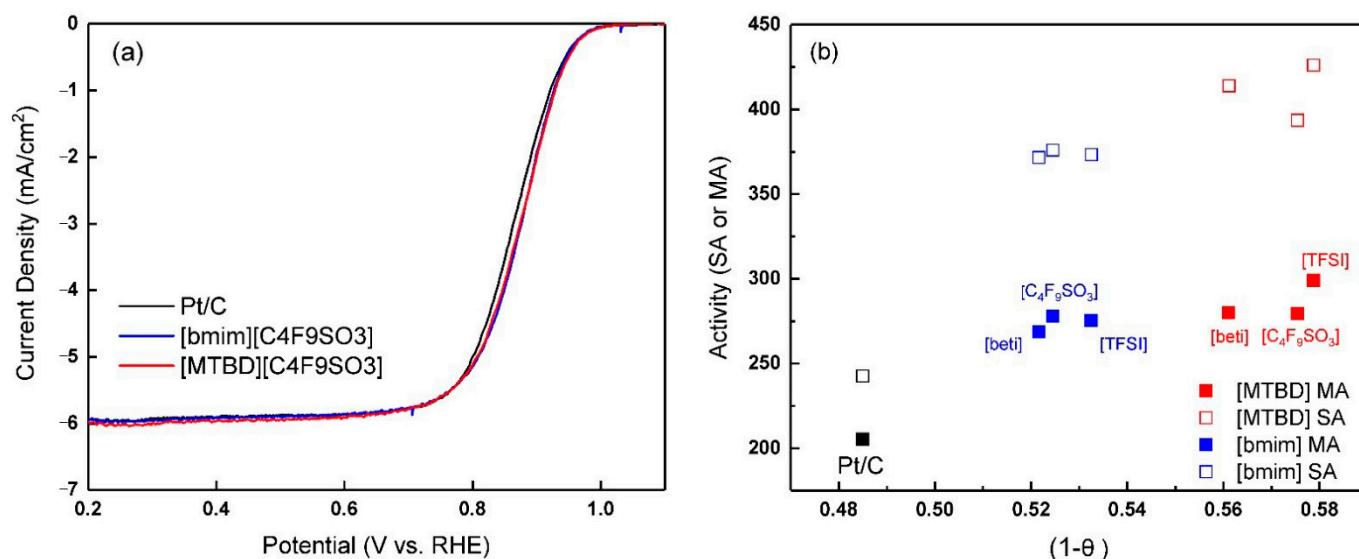


Figure 8. ORR activity measurements. (a) Polarization curves of Pt/C, Pt/C-[bmim][$\text{C}_4\text{F}_9\text{SO}_3$], and Pt/C-[MTBD][$\text{C}_4\text{F}_9\text{SO}_3$]. (b) plots of Mass activity (MA, $\text{mA}/\text{mg}_{\text{Pt}}$) and Specific activity (SA, $\mu\text{A}/\text{cm}^2_{\text{Pt}}$) as a function of $(1 - \theta)$.

The generally accepted kinetic ORR current expression form follows the equation [11,33]

$$i = nFK[\text{O}_2](1 - \theta) \exp\left(\frac{-\beta FE}{RT}\right) \exp\left(\frac{-\omega\theta}{RT}\right)$$

where the term $(1 - \theta)$ is the availability of metallic Pt. Here, we used the anodic charge as total amount of formed oxides to assess θ (θ is a ratio of anodic charge builds at 0.9 V to the

charge under H_{upd} region $\theta = \frac{Q_{\text{Oxide}}}{Q_{H_{\text{upd}}}}$ [12]. The individual values of $(1 - \theta)$ of $[\text{MTBD}]^+$ ILs were close to each other, but higher than $[\text{bmim}]^+$ ILs, as shown in Figure 8b.

Our previous studies reported that although the oxygen solubility in ILs is several fold higher than in the aqueous electrolyte, its effect on the specific ORR activity (SA) is small [12]. On the other hand, SA of Pt/C-ILs showed a dependence on $(1 - \theta)$. Figure 8b plots the ORR activities against $(1 - \theta)$. The results showed that the individual SA of Pt/C with the $[\text{MTBD}]^+$ ILs is identical but higher than those of Pt/C with $[\text{bmim}]^+$ ILs, following a similar trend of $(1 - \theta)$. Therefore, we propose that although the anion structure affects the reversible Pt-OH_{ads} formation, the eventual intrinsic activity is largely dependent on the availability of oxides-free Pt. The mass activity (MA) is a product of specific activity and electrochemical surface area. The smaller SA of Pt/C with $[\text{bmim}]^+$ ILs is compensated by the larger ECA, yielding identical mass activities of Pt/C with $[\text{MTBD}]^+$ ILs.

Besides the OH_{ads} formation, the IL anion adsorption on Pt was also reported to reduce the ORR activity [22,30]. Munakata et al. used in-situ FT-IR spectroscopy to study the anion adsorption phenomena in the pure IL electrolytes [34]. The results showed that $[\text{TFSI}]^-$ strongly adsorbed on the Pt surface through the $-\text{SO}_2-\text{N}$ group, while bulkier $[\text{beti}]^-$ exhibited a much weaker adsorption due to its extended fluoroalkyl chain. As a result, $[\text{TFSI}]^-$ exhibits a higher overpotential than $[\text{beti}]^-$. Ejigu et al. also reported that the adsorption of $[\text{TFSI}]^-$ significantly decreased the ORR activity [35]. Regarding the adsorption of $[\text{C}_4\text{F}_9\text{SO}_3]^-$, our previous results showed that it has a weak interaction with Pt and did not affect the ORR activity and ECA [12]. All those studies used a polycrystalline Pt disk immersed in the IL electrolytes. However, for the Pt-ILs studied here, Pt was exposed to abundant aqueous electrolyte, ionomer ($-\text{SO}_3\text{H}$), and ILs. Although CO displacement study has evidenced the adsorption of IL anion on Pt, based on the experimental results, it is assumed that the effect of IL anions adsorption on the ORR activity is small.

$[\text{MTBD}][\text{C}_4\text{F}_9\text{SO}_3]$ was selected for further study in the MEA. The polarization curves for Pt/C and Pt/C- $[\text{MTBD}][\text{C}_4\text{F}_9\text{SO}_3]$ were shown in Figure 9a. Compared to Pt/C, the addition of 18wt.% $[\text{MTBD}][\text{C}_4\text{F}_9\text{SO}_3]$ reduced the overall $I-V$ performance. Moreover, a significant potential drop in the high current density region was found, where oxygen transport plays a dominant role. The high current performance is strongly dependent on the electrode roughness factor ($\text{cm}^2_{\text{Pt}}/\text{cm}^2_{\text{electrode}}$) [36], and it is believed that the decreased ECA of Pt/C- $[\text{MTBD}][\text{C}_4\text{F}_9\text{SO}_3]$ is one of the major causes for the performance loss. In addition, the relatively high IL loading (18 wt.% IL) in the catalyst layer may block the pores of electrode, resulting in the increase of oxygen transport resistance.

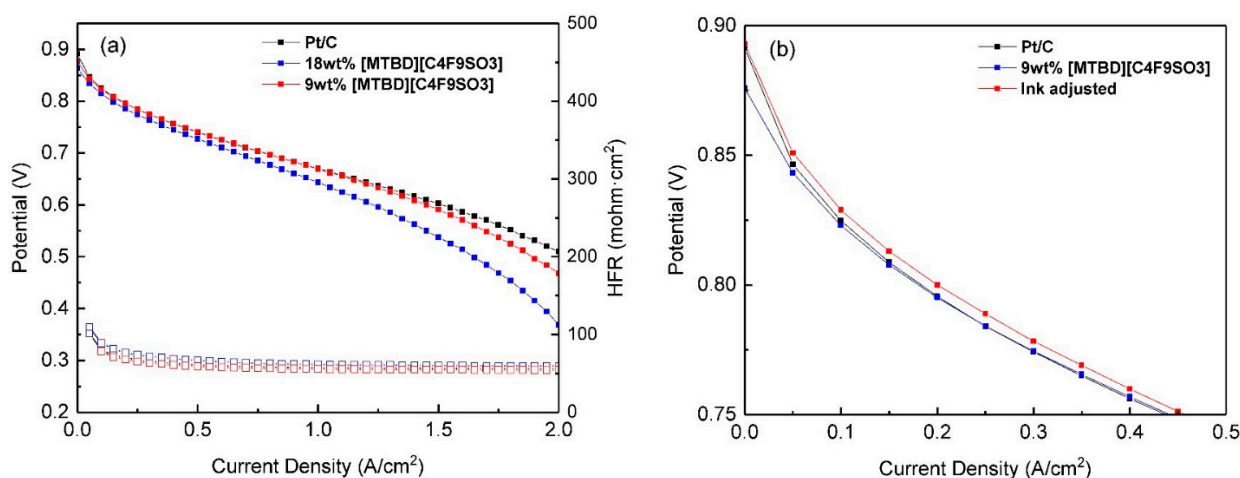


Figure 9. Polarization curves of (a) Comparison of Pt/C, Pt/C- $[\text{MTBD}][\text{C}_4\text{F}_9\text{SO}_3]$ (18 wt.% and 9 wt.% IL loading). (b) Comparison of Pt/C, Pt/C- $[\text{MTBD}][\text{C}_4\text{F}_9\text{SO}_3]$ (9 wt.%), and Pt/C- $[\text{MTBD}][\text{C}_4\text{F}_9\text{SO}_3]$ (9 wt.%) after adjustment of ink formulation (red curve). All MEA results were obtained at 70 °C and 100 RH under gauge pressure of 150 kPa.

The RDE measurements of Pt/C-ILs were conducted in fully flooded environment, where ILs experienced substantial leaching at the initial step [12]. As a result, the final IL on the catalyst surface was undoubtedly much lower than the initial value and the ORR activity enhancement solely benefited from the remaining IL. When the operation of the MEA was not in a fully flooded condition, the leaching of IL is expected to be slower than in the aqueous electrolyte. As a result, the excess of IL was responsible for the performance loss. Reducing the IL loading in half (9 wt.% IL), the performance loss in the kinetic region was largely recovered, but still inferior to Pt/C. The ORR activity improvement demonstrated in the RDE was not successfully translated into MEA. It is important to point out that IL would re-dissolve into the alcohol during the ink preparation and ORR activity improvement in the RDE was not achieved in an alcohol rich ink formula (not shown here). Therefore, in this work, we adopted a water rich ink for the RDE measurement (water to IPA volume ratio: 4/2.25). For the MEA ink slurry formulation, the water/alcohol weight ratio was set at 0.84, which may re-dissolve some of the IL. Moreover, the aggressive and extensive agitation further accelerates the IL re-dissolution, leading to a random distribution of IL in the final electrode. As a countermeasure, the water/alcohol weight ratio was adjusted to 1.33 and the MEA performance in the kinetic region was improved, as shown in Figure 9b. The finding suggests that the ink formula is critical and is worthy of further studies.

The potential loss in the high current region was not fully recovered even after adjusting IL loading and ink formula, and it leads us to consider the effect of catalyst properties such as carbon support. The carbon structures are important for the electrode design and they affect the MEA performance [37]. Therefore, in addition to the Pt/Vulcan used in this study, we also studied Pt on Ketjen black (47 wt.% Pt, TKK TEC10E50E). Different from Pt/Vulcan, which uses a solid carbon and has low surface area (~250 m²/g), Pt/Ketjen features a porous structure and high surface area (~800 m²/g). The same MEA preparation process and measurements were applied to TKK Pt/C and TKK Pt/C-[MTBD][C₄F₉SO₃], and the IL to carbon weight ratio (IL/C) was set at 0.1, the same as Pt/Vulcan-[MTBD][C₄F₉SO₃] (9 wt.% IL or IL/C = 0.1). The ink for TKK Pt/C-[MTBD][C₄F₉SO₃] was also formulated to be water rich with a water/alcohol weight ratio of 1.26. The two cathode materials exhibited identical CV profiles in the potential range, and ECAs of Pt/C-[MTBD][C₄F₉SO₃] and Pt/C were measured to be 47.3 m²/g_{Pt} and 48.7 m²/g_{Pt}, as shown in Figure 10a. It is speculated that the high surface of TKK Pt/C reduces the thickness of the IL layer compared to Pt/Vulcan at the same IL/C ratio, resulting in a minimal ECA loss. Meanwhile, IL reduced the oxides coverage of Pt/C from $\theta = 0.74$ to $\theta = 0.67$ of Pt/C-[MTBD][C₄F₉SO₃], agreeing with the CV findings in the RDE. The polarization performances of the two cathode materials were further assessed in pure O₂ to study the effect of IL on the ORR kinetics. As shown in Figure 10b, Pt/C-[MTBD][C₄F₉SO₃] exhibited a higher performance than Pt/C, and the ORR activities at 0.9 V were calculated to be 242 mA/mg_{Pt} and 179 mA/mg_{Pt}, respectively. Less oxide formation on Pt/C-IL was assumed to be one of the reasons for the activity improvement. Besides, the possibility that IL increases O₂ collision frequency and decreases anion adsorption cannot be excluded and needs further investigation. The polarization curves in air were also measured and are shown in Figure 10c. Compared to Pt/C, Pt/C-[MTBD][C₄F₉SO₃] exhibited a considerable performance increase throughout the current density range. The higher potential of Pt/C-[MTBD][C₄F₉SO₃] than Pt/C in the kinetic region can be attributed to the enhanced ORR activity. More importantly, the performance of Pt/C-[MTBD][C₄F₉SO₃] in the high current density region was greatly improved, which is believed to be associated with facilitated oxygen transport within the electrode. In general, the oxygen transport resistance in the electrode mainly consists of the molecular diffusion resistance in the pores and the transport resistance at the interface between the ionomer and Pt [38–41]. It is likely that IL reduced the oxygen transport resistance by homogeneously distributing the ionomer in the electrode [42,43] or increasing the oxygen permeability at the interface of Pt and ionomer [40]. In addition, the hydrophobic IL may limit the product water build up that hinders the mass transport of

O₂ [10]. The experimental measurements of O₂ transport resistance using an internally established method [38,39] are ongoing to explore the mechanism.

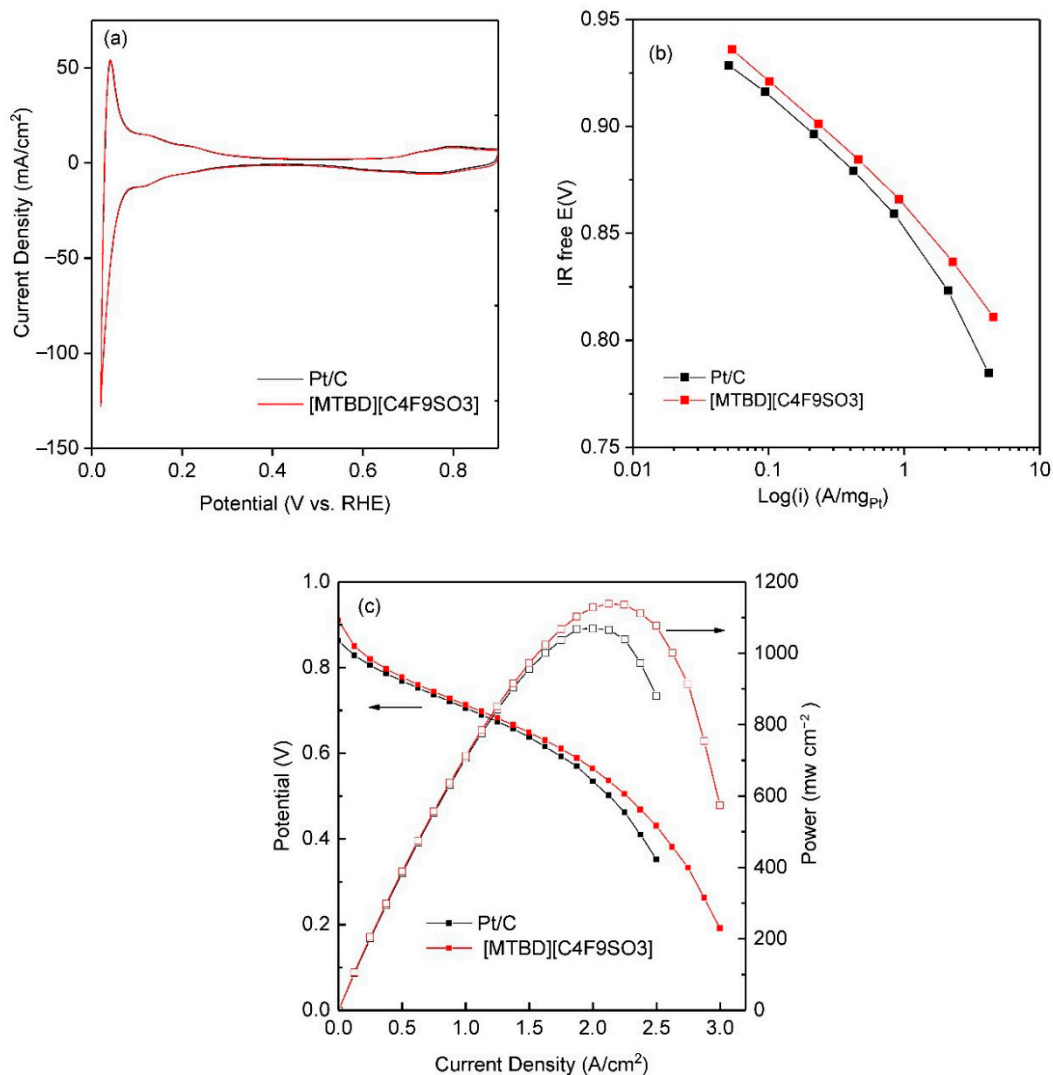


Figure 10. Electrochemical characterizations of Pt/C (TKK) and Pt/C(TKK)-[MTBD][C₄F₉SO₃] (IL/C = 0.2) in MEA. (a) cyclic voltammograms measured at 100% RH under H₂/N₂. (b) ORR polarization curves collected at 100% RH in H₂/O₂ at 100% RH under 100 kPa (abs.) (c) Polarization curves obtained in H₂/Air at 70 °C and 100 RH under gauge pressure of 150 kPa.

The MEA results reported here are far from optimized and a deeper understanding is needed to address many unknowns. More studies are underway in our laboratory including electrode engineering and we will report them in the near future. Fortunately, this study successfully demonstrated the feasibility of the application of IL to enhance the MEA performance, which may serve as a complementary solution to improve the PEMFC performance, in addition to the development of novel catalysts.

3. Experimental

Reagents. For IL synthesis, HNO₃ (70%), lithium bis((trifluoromethyl)sulfonyl) amide (99.95%), 1-butyl-3-methylimidazolium bromide, potassium nonafluorobutane sulfonate (98%) and MTBD (98%) were purchased from Sigma Aldrich (St. Louis, MO, USA). Lithium bis((perfluoroethyl)sulfonyl)amide (99%) was purchased from Iolitec (Tuscaloosa, AL, USA). For electrochemical evaluation, Johnson Matthey Pt/C catalyst (20 wt.%, Hispec 3000, Vulcan carbon as the support) was purchased from The Fuel Cell Store (College

Station, TX, USA) and used as the ORR catalyst platform for most of the RDE and MEA investigations. An additional Pt/C catalyst (TKK TEC-10E50E, Ketjen black as the support) was purchased from TANAKA Kikinzoku International (America), Inc. (Chicago, IL, USA) for the MEA study. HClO₄ (70%, GFS Chemicals (Powell, OH, USA)), isopropanol (99.5%, Sigma Aldrich (St. Louis, MO, USA)), ethanol (≥99.5%, Sigma Aldrich), propylene glycol (99.5%, Sigma Aldrich), Nafion dispersion (DE520 and D2020, Ion Power (New Castle, DE, USA)), and Nafion membrane (NR211, Ion Power) were used as received.

Synthesis of ILs: 7-methyl-1,5,7-triazabicyclo[4.4.0]dec-5-ene bis(perfluoroethylsulfonyl)amide ([MTBD][beti]): A solution of MTBD (2.51 g, 0.0164 mol) in water (100 mL) was cooled down to 0 °C and nitric acid (1.47 g, 0.0164 mol) was added dropwise to the solution, followed by the addition of lithium bis(perfluoroethylsulfonyl)amide (6.34 g, 0.0164 mol). The mixture was stirred for 1 h and the IL was separated from the mixture as a viscous fluid phase beneath the aqueous phase. The resulting IL was washed 4 times with ultrapure water and dried under reduced pressure on a rotary evaporator at 50 °C for 18 h to obtain a colorless liquid.

Similar synthesis routes and purification processes were used to prepare the rest of the ILs:

7-methyl-1,5,7-triazabicyclo[4.4.0]dec-5-ene bis(trifluoromethylsulfonyl)amide ([MTBD][TFSI]).—The chemicals used to prepare [MTBD][TFSI] were: MTBD (2.25 g, 0.0146 mol), nitric acid (1.32 g, 0.0146 mol), and lithium bis((trifluoro- methyl)sulfonyl)amide (4.22 g, 0.0146 mol).

7-methyl-1,5,7-triazabicyclo[4.4.0]dec-5-ene 1,1,2,2,3,3,4,4,4-nonafluorobutane-1-sulfonate ([MTBD][C₄F₉SO₃]).—The chemicals used to prepare [MTBD][C₄F₉SO₃] were: MTBD (3.00 g, 0.0196 mol), nitric acid (1.76 g, 0.0196 mol) and potassium nonafluorobutane sulfonate (8.58 g, 0.0196 mol).

1-butyl-3-methylimidazolium bis(perfluoroethylsulfonyl)amide ([bmim][beti]).—The chemicals used to prepare [bmim][beti] were [bmim][Br] (3.50 g, 0.0159 mol) and lithium bis((perfluoroethyl)sulfonyl)amide (6.18 g, 0.0159 mol).

1-butyl-3-methylimidazolium bis(trifluoromethylsulfonyl)amide ([bmim][TFSI]).—The chemicals used to prepare [bmim][TFSI] were: [bmim][Br] (3.5 g, 0.0159 mol) and lithium bis(trifluoro- methylsulfonyl)amide (4.59 g, 0.0159 mol).

1-butyl-3-methylimidazolium 1,1,2,2,3,3,4,4,4-nonafluorobutane-1-sulfonate ([bmim][C₄F₉SO₃]).—The chemicals used to prepare [bmim][C₄F₉SO₃] were: [bmim][Br] (3.00 g, 0.0136 mol) and potassium nonafluorobutane sulfonate (4.63 g, 0.0136 mol).

ATR-FTIR measurements. ATR-FTIR spectra of synthesized ionic liquid were recorded using a Thermo Scientific Nicolet™ iS20 FTIR (Thermo Fisher Scientific, Waltham, MA, USA) Spectrometer in the range 400–4000 cm^{−1}.

Contact angle measurements: The contact angles of ILs on Pt film and carbon surfaces were measured with a Drop Shape Analyzer DSA100S (KRÜSS Scientific Instruments, Inc., Matthews, NC, USA). Platinum was deposited on a wafer by sputter coating (Intlvac, Fort Collins, CO, USA) with a thickness of 250 nm. A glassy carbon plate (25 × 25 mm, type 2) was purchased from Alfa Aesar (Tewksbury, MA, USA) and used as received without further polishing. The substrates were washed sequentially with isopropanol and deionized water in an ultrasonic bath for 30 min and dried in air. An environmental chamber TC11 (KRÜSS Scientific Instruments, Inc., Matthews, NC, USA) was saturated with dry nitrogen and the temperature was controlled at 20 ± 0.1 °C. A 1 µL sample of IL was dispensed onto the substrate surface and equilibrated for 10 min until the contact angle no longer changed. Then a final measurement was taken to record the contact angle. Five independent measurements were taken for each IL on each substrate and the average of the measurements was obtained. The overall uncertainties for contact angles are the standard deviations calculated from the data for five independent drops. The solid substrates were scanned using an Asylum MFP-3D atomic force microscope (AFM) (Oxford Instruments NanoAnalysis & Asylum Research, High Wycombe, UK) on three random locations using 50 µm × 50 µm scan sizes. The roughness was analyzed with the internal

software provided by Asylum Research for calculating the root mean square (RMS) and arithmetic average (Ra). The roughness of the glassy carbon is 0.88 nm (RMS) and 0.48 nm (Ra). The roughness of the platinum is 1.93 nm (RMS) and 1.46 nm (Ra).

ORR activity measurements. All electrochemical measurements were performed on an EC-LAB SP-300 (BioLogic Science Instruments, Knoxville, TN) and the electrolytes were prepared with Millipore (Milli-Q Synthesis, Millipore Sigma, Burlington, MA) water with a resistance greater than 18.2 M Ω ·cm. A Pt wire (Pine Research Instrumentation, Inc. (Durham, NC), AFCTR5) and a hydrogen reference electrode (Hydroflex, eDAQ) were used as counter electrode and reference electrode, respectively. All potentials in this work are reported against a reversible hydrogen electrode (RHE) unless specified otherwise.

The details of preparation of IL impregnated Pt/C (Pt/C-ILs) can be found in our previous publication [12]. Here, the IL loading was controlled at 18 wt.%, much lower than the previous study. The Pt/C-IL was dispersed in a solution containing 4 mL DI water, 2.25 mL isopropanol and 25 μ L Nafion dispersion (DE520) and the ink was subject to 15 min ultrasonication in an ice bath. A 10 μ L aliquot of this ink was pipetted onto the glassy carbon (GC) disk (5 mm diameter, Pine Instrument) and rotationally dried in air to form a uniform catalyst layer [44]. The calculated final Pt loading on the disk is 16.2 μ g/cm²_{disk}. The control sample of Pt/C without IL was prepared in the exact same way as the Pt/C-IL samples.

The catalyst coated GC was first pre-conditioned in N₂-saturated 0.1 M HClO₄. Typically, the working disk was scanned from 0.05 V to 1.2 V with a scan rate of 100 mV·s⁻¹ until the cyclic voltammetry (CV) curve did not change. After that, a stable CV was recorded from 0.05 to 1.2 V at 50 mV·s⁻¹. ECA_(H_{upd}) was obtained by integrating the charge under the hydrogen adsorption region (H_{upd}). ORR measurements were conducted in the saturated 0.1 M HClO₄ and multiple independent data sets were collected. All the intrinsic activities were corrected with N₂-background and IR compensation [12].

CO measurements. CO stripping experiment was carried out to estimate the ECA_(CO) of Pt/C-ILs, which was compared with ECA_(H_{upd}). In general, CO (2% carbon monoxide in argon, Airgas) was introduced into N₂ pre-saturated 0.1 M HClO₄ while holding the electrode potential at 0.1 V for 15 min to complete the CO adsorption on the Pt surface. Then the electrolyte was purged with N₂ for 20 min to remove the CO while maintaining the electrode potential at 0.1 V. The adsorbed monolayer of CO on the Pt surface was then stripped off by sweeping the electrode from 0.1 V to 1.2 V for 3 cycles at a scan rate of 20 mV·s⁻¹. The second cycle was used as baseline for the CO stripping peak in the first cycle and the charge under the peak was integrated for the ECA_(CO) calculation, assuming a specific charge of 420 μ C cm_{Pt}⁻² for a monolayer of adsorbed CO [16].

CO displacement characterization was employed to investigate the effect of IL structure on the surface coverage in the Pt/C-ILs. Typically, the catalyst coated electrode was immersed in N₂-saturated 0.1 M HClO₄ and conditioned by cycling 80 times from 0.05 to 1.2 V. Then the electrode was held at a desired potential (e.g., 0.5 V) and the N₂ valve was switched to CO gas. A displacement current was recorded until a new baseline was established and the charge under the curve was integrated as the displacement charge of either anion or cation adsorbed on the Pt surface [15].

MEA preparation. The Pt/C-[MTBD][C₄F₉SO₃] was selected as cathode material for the MEA evaluation, and compared with Pt/C. The catalyst ink consisted of ethanol, propylene glycol, water, Nafion ionomer (D2020), and catalyst. The ionomer to carbon (I/C) weight ratio and the solid content were kept at 0.9 and 14 wt.%, respectively. The ink slurry was vigorously mixed and coated on a poly (tetrafluoro-ethylene) substrate (0.002" thick, McMaster-CARR) using a doctor-blade casting method. Similarly, a Pt/C (30 wt.% Pt/C, TEC10EA30E, TKK) catalyst layer with I/C ratio at 1.07 was prepared as the anode material. The coating layer was dried at 80 °C to remove the solvent. The final anode and cathode Pt loading were controlled at 0.05 and 0.16 mg_{Pt}/cm², respectively. Two pieces of square electrocatalyst layer (2 cm × 2 cm) of cathode and anode were punched and sandwiched between a Nafion 211 membrane to form a catalyst coated membrane (CCM) using a

decal-transfer technique [45]. The hot-pressing condition was set at 130 °C and 0.8 MPa for 5 min. The gas diffusion layers (29 BC, SGL Carbon (Charlotte, NC)) together with the CCM were assembled in a single cell with a serpentine flow field (Scribner Associates, Southern Pines, NC, USA).

MEA measurements: A 850e Fuel Cell test system (Scribner Associates) was used for the MEA performance evaluation. The MEA was first activated by sweeping between 0.9 V and 0.1 V for several hundred cycles under H₂/Air (0.5 NLPM/1 NLPM) at 45 °C and relative humidity (RH) of 100%. Then the i-V performance of the MEAs were measured at 70 °C under 100% RH. Ultrapure H₂ and Air were supplied to the anode and cathode with a gauge pressure of 150 kPa. The current density was set with an incremental of 0.05 A/cm² and the response voltage was recorded simultaneously. The high frequency resistance (HFR) was also recorded throughout the measurement.

4. Conclusions

We have examined a series of ILs to study the effects of cation and anion on the oxygen reduction reaction. Several combinations of ILs were designed and systematically studied. The incorporation of IL reduced the Pt-oxides coverage and anion adsorption, mainly by decreasing the exposure of Pt to the electrolyte and ionomer. Moreover, the decrease of side reactions contributed to the improved ORR activities. Meanwhile, it was found that the effect of the cation on the electrochemical performance was more pronounced than the anion, and [MTBD]⁺ ILs showed higher influences than [bmim]⁺ ILs, presumably owing to the stronger interaction with the catalyst. In addition to the investigation in the RDE, studies were also extended to the MEA. It was found that the catalyst ink formulation and the catalyst property were important to translate the benefits of the IL from the RDE to the MEA. Using a water rich ink and a high surface area catalyst, considerable MEA performance improvement of Pt/C-IL was successfully demonstrated. This study suggests the importance of IL structure and it can be expected that the development of new ILs would contribute to the continuous performance improvement of Pt(alloy)-IL systems.

Supplementary Materials: The following are available online at <https://www.mdpi.com/article/10.3390/catal11080989/s1>, Figures S1–S16: NMR Spectra of the ILs synthesized in this study.

Author Contributions: Conceptualization, K.H., H.J. and J.F.B.; IL synthesis and characterization, O.M.-C., Z.C. and T.S.; IL-impregnation and electrochemical experiments, K.H.; writing—original draft preparation, K.H.; writing—review and editing, L.W., H.L., J.F.B. and H.J.; supervision, J.F.B. and H.J. All authors have read and agreed to the published version of the manuscript.

Funding: This research receives no external funding.

Conflicts of Interest: The authors declare no conflict of interest.

References

1. Papageorgopoulos, D. U.S. Department of Energy Office of Energy Efficiency & Renewable Energy 2021 Annual Merit Review and Peer Evaluation Meeting, Fuel Cell Technologies Overview. 2021. Available online: www.hydrogen.energy.gov/pdfs/review21/plenary8_papageorgopoulos_2021_o.pdf (accessed on 23 July 2021).
2. Huang, L.; Zaman, S.; Tian, X.; Wang, Z.; Fang, W.; Xia, B.Y. Advanced Platinum-Based Oxygen Reduction Electrocatalysts for Fuel Cells. *Acc. Chem. Res.* **2021**, *54*, 311–322. [[CrossRef](#)] [[PubMed](#)]
3. Tian, X.; Lu, X.F.; Xia, B.Y.; Lou, X.W. Advanced Electrocatalysts for the Oxygen Reduction Reaction in Energy Conversion Technologies. *Joule* **2020**, *4*, 45–68. [[CrossRef](#)]
4. Liu, Z.; Zhao, Z.; Peng, B.; Duan, X.; Huang, Y. Beyond Extended Surfaces: Understanding the Oxygen Reduction Reaction on Nanocatalysts. *J. Am. Chem. Soc.* **2020**, *142*, 17812–17827. [[CrossRef](#)]
5. Snyder, J.; Fujita, T.; Chen, M.; Erlebacher, J. Oxygen reduction in nanoporous metal–ionic liquid composite electrocatalysts. *Nat. Mater.* **2010**, *9*, 904–907. [[CrossRef](#)]
6. Chen, C.; Kang, Y.; Huo, Z.; Zhu, Z.; Huang, W.; Xin, H.L.; Snyder, J.D.; Li, D.; Herron, J.A.; Mavrikakis, M.; et al. Highly Crystalline Multimetallic Nanoframes with Three-Dimensional Electrocatalytic Surfaces. *Science* **2014**, *343*, 1339–1343. [[CrossRef](#)] [[PubMed](#)]
7. Zhang, G.-R.; Munoz, M.; Etzold, B.J. Boosting Performance of Low Temperature Fuel Cell Catalysts by Subtle Ionic Liquid Modification. *ACS Appl. Mater. Interfaces* **2015**, *7*, 3562–3570. [[CrossRef](#)]

8. Zhang, G.-R.; Munoz, M.; Etzold, B.J.M. Accelerating Oxygen-Reduction Catalysts through Preventing Poisoning with Non-Reactive Species by Using Hydrophobic Ionic Liquids. *Angew. Chem. Int. Ed.* **2015**, *55*, 2257–2261. [[CrossRef](#)]
9. George, M.; Zhang, G.-R.; Schmitt, N.; Brunnengräber, K.; Sandbeck, D.J.S.; Mayrhofer, K.; Cherevko, S.; Etzold, B.J.M. Effect of Ionic Liquid Modification on the ORR Performance and Degradation Mechanism of Trimetallic PtNiMo/C Catalysts. *ACS Catal.* **2019**, *9*, 8682–8692. [[CrossRef](#)] [[PubMed](#)]
10. Snyder, J.D.; Livi, K.J.T.; Erlebacher, J. Oxygen Reduction Reaction Performance of [MTBD][beti]-Encapsulated Nanoporous NiPt Alloy Nanoparticles. *Adv. Funct. Mater.* **2013**, *23*, 5494–5501. [[CrossRef](#)]
11. Benn, E.; Uvegi, H.; Erlebacher, J. Characterization of Nanoporous Metal-Ionic Liquid Composites for the Electrochemical Oxygen Reduction Reaction. *J. Electrochem. Soc.* **2015**, *162*, H759–H766. [[CrossRef](#)]
12. Huang, K.; Song, T.; Morales-Collazo, O.; Jia, H.; Brennecke, J.F. Enhancing Pt/C Catalysts for the Oxygen Reduction Reaction with Protic Ionic Liquids: The Effect of Anion Structure. *J. Electrochem. Soc.* **2017**, *164*, F1448–F1459. [[CrossRef](#)]
13. Li, Y.; Intikhab, S.; Malkani, A.; Xu, B.; Snyder, J.D. Ionic Liquid Additives for the Mitigation of Nafion Specific Adsorption on Platinum. *ACS Catal.* **2020**, *10*, 7691–7698. [[CrossRef](#)]
14. Zhang, G.-R.; Wolker, T.; Sandbeck, D.J.S.; Munoz, M.; Mayrhofer, K.; Cherevko, S.; Etzold, B.J.M. Tuning the Electrocatalytic Performance of Ionic Liquid Modified Pt Catalysts for the Oxygen Reduction Reaction via Cationic Chain Engineering. *ACS Catal.* **2018**, *8*, 8244–8254. [[CrossRef](#)] [[PubMed](#)]
15. Garrick, T.; Moylan, T.E.; Yarlagadda, V.; Kongkanand, A. Characterizing Electrolyte and Platinum Interface in PEM Fuel Cells Using CO Displacement. *J. Electrochem. Soc.* **2016**, *164*, F60–F64. [[CrossRef](#)]
16. Binninger, T.; Fabbri, E.; Kötz, R.; Schmidt, T.J. Determination of the Electrochemically Active Surface Area of Metal-Oxide Supported Platinum Catalyst. *J. Electrochem. Soc.* **2013**, *161*, H121–H128. [[CrossRef](#)]
17. Garrick, T.; Moylan, T.E.; Carpenter, M.K.; Kongkanand, A. Editors' Choice—Electrochemically Active Surface Area Measurement of Aged Pt Alloy Catalysts in PEM Fuel Cells by CO Stripping. *J. Electrochem. Soc.* **2016**, *164*, F55–F59. [[CrossRef](#)]
18. Marković, N.M.; Lucas, C.A.; Rodes, A.; Stamenković, V.; Ross, P.N. Surface electrochemistry of CO on Pt (111): Anion effects. *Surf. Sci.* **2002**, *499*, L149–L158. [[CrossRef](#)]
19. Li, Y.; Hart, J.; Profitt, L.; Intikhab, S.; Chatterjee, S.; Taheri, M.; Snyder, J. Sequential Capacitive Deposition of Ionic Liquids for Conformal Thin Film Coatings on Oxygen Reduction Reaction Electrocatalysts. *ACS Catal.* **2019**, *9*, 9311–9316. [[CrossRef](#)]
20. Li, Y.; Van Cleve, T.; Sun, R.; Gawas, R.; Wang, G.; Tang, M.H.; Elabd, Y.A.; Snyder, J.D.; Neyerlin, K.C. Modifying the Electrocatalyst–Ionomer Interface via Sulfonated Poly(ionic liquid) Block Copolymers to Enable High-Performance Polymer Electrolyte Fuel Cells. *ACS Energy Lett.* **2020**, *5*, 1726–1731. [[CrossRef](#)]
21. Arras, J.; Paki, E.; Roth, C.; Radnik, J.; Lucas, M.; Claus, P. How a Supported Metal Is Influenced by an Ionic Liquid: In-Depth Characterization of SCILL-Type Palladium Catalysts and Their Hydrogen Adsorption. *J. Phys. Chem. C* **2010**, *114*, 10520–10526. [[CrossRef](#)]
22. Markovic, N.; Gasteiger, H.; Ross, P.N. Kinetics of Oxygen Reduction on Pt(hkl) Electrodes: Implications for the Crystallite Size Effect with Supported Pt Electrocatalysts. *J. Electrochem. Soc.* **1997**, *144*, 1591–1597. [[CrossRef](#)]
23. Arras, J.; Steffan, M.; Shayeghi, Y.; Ruppert, D.; Claus, P. Regioselective catalytic hydrogenation of citral with ionic liquids as reaction modifiers. *Green Chem.* **2009**, *11*, 716–723. [[CrossRef](#)]
24. Gómez, R.; Rodes, A.; Pérez, J.; Feliu, J.; Aldaz, A. Electrochemical and in situ FTIR studies of the CO adsorption at palladium and rhodium multilayers deposited on platinum single crystal surfaces. I. Pt(110) substrate. *Surf. Sci.* **1995**, *327*, 202–215. [[CrossRef](#)]
25. Clavilier, J.; Orts, J.; Gómez, R.; Feliu, J.; Aldaz, A. Comparison of electrosorption at activated polycrystalline and Pt(531) kinked platinum electrodes: Surface voltammetry and charge displacement on potentiostatic CO adsorption. *J. Electroanal. Chem.* **1996**, *404*, 281–289. [[CrossRef](#)]
26. Bergelin, M.; Herrero, E.; Feliu, J.; Wasberg, M. Oxidation of CO adlayers on Pt(111) at low potentials: An impinging jet study in H₂SO₄ electrolyte with mathematical modeling of the current transients. *J. Electroanal. Chem.* **1999**, *467*, 74–84. [[CrossRef](#)]
27. Farias, M.J.S.; Camara, G.; Feliu, J. Understanding the CO Preoxidation and the Intrinsic Catalytic Activity of Step Sites in Stepped Pt Surfaces in Acidic Medium. *J. Phys. Chem. C* **2015**, *119*, 20272–20282. [[CrossRef](#)]
28. Omura, J.; Yano, H.; Watanabe, M.; Uchida, H. Electrochemical Quartz Crystal Microbalance Analysis of the Oxygen Reduction Reaction on Pt-Based Electrodes. Part 1: Effect of Adsorbed Anions on the Oxygen Reduction Activities of Pt in HF, HClO₄, and H₂SO₄ Solutions. *Langmuir* **2011**, *27*, 6464–6470. [[CrossRef](#)]
29. Roques, J.; Anderson, A.B.; Murthi, V.S.; Mukerjee, S. Potential shift for OH (ads) formation on the Pt skin on Pt₃Co (111) electrodes in acid: Theory and experiment. *J. Electrochem. Soc.* **2005**, *152*, E193. [[CrossRef](#)]
30. Wang, J.X.; Markovic, N.M.; Adzic, R.R. Kinetic Analysis of Oxygen Reduction on Pt(111) in Acid Solutions: Intrinsic Kinetic Parameters and Anion Adsorption Effects. *J. Phys. Chem. B* **2004**, *108*, 4127–4133. [[CrossRef](#)]
31. Conway, B.E.; Barnett, B.; Angerstein-Kozłowska, H.; Tilak, B.V. A surface-electrochemical basis for the direct logarithmic growth law for initial stages of extension of anodic oxide films formed at noble metals. *J. Chem. Phys.* **1990**, *93*, 8361–8373. [[CrossRef](#)]
32. Jerkiewicz, G.; Vatankhah, G.; Lessard, J.; Soriaga, M.P.; Park, Y.-S. Surface-oxide growth at platinum electrodes in aqueous H₂SO₄: Reexamination of its mechanism through combined cyclic-voltammetry, electrochemical quartz-crystal nanobalance, and Auger electron spectroscopy measurements. *Electrochim. Acta* **2004**, *49*, 1451–1459. [[CrossRef](#)]
33. Subramanian, N.P.; Greszler, T.; Zhang, J.; Gu, W.; Makharia, R.R. Pt-Oxide Coverage-Dependent Oxygen Reduction Reaction (ORR) Kinetics. *ECS Meet. Abstr.* **2011**, *159*, B531. [[CrossRef](#)]

34. Munakata, H.; Tashita, T.; Haibara, M.; Kanamura, K. Synthesis of New Protic Ionic Liquids for Fuel Cells on the Basis of In Situ FT-IR Measurements. *ECS Trans.* **2010**, *33*, 463. [[CrossRef](#)]
35. Ejigu, A.; Walsh, D.A. The Role of Adsorbed Ions during Electrocatalysis in Ionic Liquids. *J. Phys. Chem. C* **2014**, *118*, 7414–7422. [[CrossRef](#)]
36. Kongkanand, A.; Mathias, M. The Priority and Challenge of High-Power Performance of Low-Platinum Proton-Exchange Membrane Fuel Cells. *J. Phys. Chem. Lett.* **2016**, *7*, 1127–1137. [[CrossRef](#)] [[PubMed](#)]
37. Park, Y.-C.; Tokiwa, H.; Kakinuma, K.; Watanabe, M.; Uchida, M. Effects of carbon supports on Pt distribution, ionomer coverage and cathode performance for polymer electrolyte fuel cells. *J. Power Sources* **2016**, *315*, 179–191. [[CrossRef](#)]
38. Nonoyama, N.; Okazaki, S.; Weber, A.; Ikogi, Y.; Yoshida, T. Analysis of Oxygen-Transport Diffusion Resistance in Proton-Exchange-Membrane Fuel Cells. *J. Electrochem. Soc.* **2011**, *158*, B416–B423. [[CrossRef](#)]
39. Suzuki, T.; Yamada, H.; Tsusaka, K.; Morimoto, Y. Modeling of Oxygen Diffusion Resistance in Polymer Electrolyte Fuel Cells in the Intermediate Potential Region. *J. Electrochem. Soc.* **2018**, *165*, F166–F172. [[CrossRef](#)]
40. Jinnouchi, R.; Kudo, K.; Kitano, N.; Morimoto, Y. Molecular Dynamics Simulations on O₂ Permeation through Nafion Ionomer on Platinum Surface. *Electrochim. Acta* **2016**, *188*, 767–776. [[CrossRef](#)]
41. Kodama, K.; Motobayashi, K.; Shinohara, A.; Hasegawa, N.; Kudo, K.; Jinnouchi, R.; Osawa, M.; Morimoto, Y. Effect of the Side-Chain Structure of Perfluoro-Sulfonic Acid Ionomers on the Oxygen Reduction Reaction on the Surface of Pt. *ACS Catal.* **2017**, *8*, 694–700. [[CrossRef](#)]
42. Takahashi, S.; Mashio, T.; Horibe, N.; Akizuki, K.; Ohma, A. Analysis of the Microstructure Formation Process and Its Influence on the Performance of Polymer Electrolyte Fuel-Cell Catalyst Layers. *ChemElectroChem* **2015**, *2*, 1560–1567. [[CrossRef](#)]
43. Takahashi, S.; Shimanuki, J.; Mashio, T.; Ohma, A.; Tohma, H.; Ishihara, A.; Ito, Y.; Nishino, Y.; Miyazawa, A. Observation of ionomer in catalyst ink of polymer electrolyte fuel cell using cryogenic transmission electron microscopy. *Electrochim. Acta* **2017**, *224*, 178–185. [[CrossRef](#)]
44. Shinozaki, K.; Zack, J.W.; Richards, R.M.; Pivovar, B.S.; Kocha, S.S. Oxygen reduction reaction measurements on platinum electrocatalysts utilizing rotating disk electrode technique: I. Impact of impurities, measurement protocols and applied corrections. *J. Electrochem. Soc.* **2015**, *162*, F1144. [[CrossRef](#)]
45. Iden, H.; Ohma, A.; Shinohara, K. Analysis of Proton Transport in Pseudo Catalyst Layers. *J. Electrochem. Soc.* **2009**, *156*, B1078–B1084. [[CrossRef](#)]